JACS
JOURNAL OF THE AMERICAN CHEMICAL SOCIETY

ARTICLE

pubs.acs.org/JACS

Moving Protons with Pendant Amines: Proton Mobility in a Nickel Catalyst for Oxidation of Hydrogen

Molly O'Hagan, Wendy J. Shaw,* Simone Raugei,* Shentan Chen, Jenny Y. Yang, Uriah J. Kilgore, Daniel L. DuBois, and R. Morris Bullock*

Center for Molecular Electrocatalysis, Pacific Northwest National Laboratory, P.O. Box 999, K2-57, Richland, Washington 99352, United States

Supporting Information

ABSTRACT: Proton transport is ubiquitous in chemical and biological processes, including the reduction of dioxygen to water, the reduction of CO_2 to formate, and the production/oxidation of hydrogen. In this work we describe intramolecular proton transfer between Ni and positioned pendant amines for the hydrogen oxidation electrocatalyst $[Ni(P^{Cy}_2N^{Bn}_2H)_2]^{2+}$ ($P^{Cy}_2N^{Bn}_2$ = 1,5-dibenzyl-3,7-dicyclohexyl-1,5-diaza-3,7-diphosphacyclooctane). Rate constants are determined by variable-temperature one-dimensional NMR techniques and two-dimensional EXSY experiments. Computational studies provide insight into the details of the proton movement and energetics of these complexes. Intramolecular proton exchange processes are observed for two of the three experimentally observable isomers of the doubly protonated Ni(0) complex, $[Ni(P^{Cy}_2N^{Bn}_2H)_2]^{2+}$, which have N−H bonds but no Ni−H bonds. For these two isomers, with pendant amines positioned endo to the Ni, the rate constants for proton exchange range from 10^4 to 10^5 s^{-1} at 25 °C, depending on isomer and solvent. No exchange is observed for protons on pendant amines positioned exo to the Ni. Analysis of the exchange as a function of temperature provides a barrier for proton exchange of $\Delta G^{\ddagger}$ = 11−12 kcal/mol for both isomers, with little dependence on solvent. Density functional theory calculations and molecular dynamics simulations support the experimental observations, suggesting metal-mediated intramolecular proton transfers between nitrogen atoms, with chair-to-boat isomerizations as the rate-limiting steps. Because of the fast rate of proton movement, this catalyst may be considered a metal center surrounded by a cloud of exchanging protons. The high intramolecular proton mobility provides information directly pertinent to the ability of pendant amines to accelerate proton transfers during catalysis of hydrogen oxidation. These results may also have broader implications for proton movement in homogeneous catalysts and enzymes in general, with specific implications for the proton channel in the Ni−Fe hydrogenase enzyme.

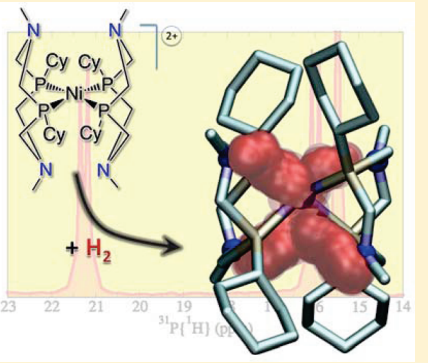

INTRODUCTION

The controlled movement of protons is essential in many biological transformations. Cytochrome c-oxidase,[1,2] gramicidin A,[3,4] and carbonic anhydrase II[5] are well-known examples of enzymes that move protons easily over large distances. Hydrogenases[6−10] are another example of a family of enzymes that move protons efficiently; they have received substantial attention in recent years due to interest in the production or oxidation of hydrogen for energy storage and use. The bimetallic active site and outer-coordination sphere of these enzymes[6,11,12] have evolved to control the efficient formation or cleavage of the H−H bond and facilitate proton transfer between the metal center and proton relays within the protein matrix during the catalytic cycle. However, studying proton movement at a molecular level within these enzymes is challenging due to their size and complexity, and the exquisite studies that are done often require many mutations to indirectly identify the proton channel.[6]

A significant advance in understanding proton movement in hydrogenases was made when the crystal structure of the Fe−Fe hydrogenase revealed a dithiolate bridge that is widely accepted to contain an amine, positioned properly to transfer protons to and from the distal Fe (**1**).[13−15]

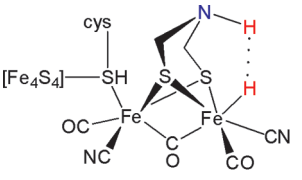

1

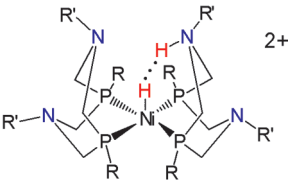

2

These considerations and others led our laboratories to develop $Ni(P^R_2N^{R'}_2)_2^{2+}$ electrocatalysts containing 1,5-diaza-3,7-diphosphacyclooctane ($P^R_2N^{R'}_2$) ligands that provide positioned

Received: February 28, 2011
Published: May 19, 2011

pendant amines in the second coordination sphere to facilitate proton movement (**2**).[16−25] The pendant amine has been demonstrated to be necessary for the fast rates observed for hydrogen production[23−25] (up to 1850 s^{-1} at 22 °C),[26] exceeding those of the Ni−Fe hydrogenase (700 s^{-1} at 30 °C).[27] The simplicity of these catalysts and their similarity with the enzyme active site provide an opportunity to investigate proton movement to and from the metal at a molecular level, with implications for both enzymatic systems and organometallic catalysts involved in multi-proton and multi-electron reactions.

We have chosen $[Ni(P^{Cy}_2N^{Bn}_2)_2]^{2+}$, a catalyst for the oxidation of hydrogen (Cy = cyclohexyl, Bn = benzyl),[20] to investigate intramolecular proton transfer. This catalyst was chosen because it allows the direct observation of many of the proposed reaction intermediates using experimental NMR techniques. Addition of H_2 to $[Ni(P^{Cy}_2N^{Bn}_2)_2]^{2+}$ has been shown to produce $[Ni(P^{Cy}_2N^{Bn}_2H)_2]^{2+}$, a Ni^0 complex with two protonated amines.[21] Characterization of $[Ni(P^{Cy}_2N^{Bn}_2H)_2]^{2+}$ by ^1H, ^{31}P, and ^{15}N NMR revealed that this complex exists as three isomers, **A**, **B**, and **C**, that differ in the orientation of the N−H bonds.

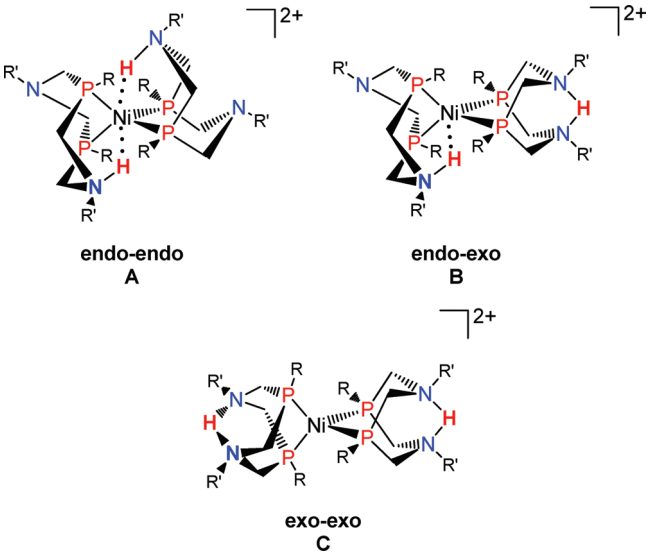

Isomer **A** has both N−H bonds endo to the nickel, while isomer **C** has both N−H bonds exo to the nickel, in a "pinched" (N−H−N) configuration. Isomer **B** has a mixed endo-exo geometry. Based on the structure and the proposed mechanism for H_2 production and oxidation for $[Ni(P^R_2N^{R'}_2)_2]^{2+}$ catalysts,[23−26,34] only pendant amines having an endo geometry are properly positioned to function efficiently as proton relays during catalysis, as demonstrated by complexes **1** and **2**. In order to provide detailed mechanistic insight on how these intramolecular proton transfer reactions occur, we report combined experimental and computational studies for $[Ni(P^{Cy}_2N^{Bn}H)_2]^{2+}$, a catalytic intermediate for the oxidation of hydrogen.

RESULTS AND ANALYSIS

Proton Exchange Rates for $[Ni(P^{Cy}_2N^{Bn}_2H)_2]^{2+}$. To gain a better understanding of the nature of the exchange processes occurring for isomers **A**−**C**, $^{31}P\{^1H\}$ NMR spectra of $[Ni(P^{Cy}_2N^{Bn}_2H)_2]^{2+}$ in CD_3CN were recorded from −40 to 50 °C, in 10 °C increments (20 °C increments shown in Figure 1 for clarity). Consistent with previous results,[21] the spectrum for **A** at −40 °C shows resonances at 21.2 and 16.0 ppm. The observation of two ^{31}P chemical shifts for this isomer is attributed to two of the phosphorus atoms being adjacent to an N−H group in a boat conformation, while the other two are not spatially near an amine. Similarly, the phosphorus atoms of the exo-protonated ligand of isomer **B** have chemical shifts at −5.8 and −10.2 ppm, depending on the orientation relative to the protonated amine on the opposite ligand. The phosphorus atoms on the endo-protonated ligand of isomer **B** have equivalent chemical shifts (15.5 ppm), as do the phosphorus atoms in isomer **C** (−11.0 ppm).[28] The additional splitting observed on the resonances for **A**, as well as for the exo portion of **B**, is due to the inequivalence of the phosphorus atoms, creating AA′BB′ splitting patterns.

The multiple narrow ^{31}P NMR resonances for complexes **A** and **B** at −40 °C indicate that exchange processes are very slow at this temperature. The resonances for isomers **A** and **B** begin to broaden at about −20 °C, indicating an increased rate of exchange. The coalescence temperature for **B** is ∼0 °C; at 20 °C, this resonance has begun to narrow again as it approaches the fast exchange limit. A slightly different temperature regime is observed for **A**, where coalescence occurs at ∼10 °C. At 20 °C, this resonance is still very broad, indicating that the fast exchange limit has not yet been reached. The downfield resonance for **B** and the resonance for **C** remain sharp throughout the temperature range, likely indicating the absence of exchange on the NMR time scale, although rapid exchange would look similar. The variable-temperature spectra for $[Ni(P^{Cy}_2N^{Bn}_2H)_2]^{2+}$ in acetone and methylene chloride are similar to those observed in acetonitrile (Figures S1 and S2 in the Supporting Information).

The NMR data were modeled using a two-site exchange process, shown schematically in Figure 2; representative fits are shown in Figure S3.[29] The rate constants for exchange as functions of temperature and solvent are shown in Table 1, ranging from about 10^4 to 10^5 s^{-1} at room temperature for both isomers **A** and **B**. Activation parameters were determined by fitting the variable-temperature data covering the temperature range of −40 to 50 °C (Figures 3 and S4). The resulting activation parameters as a function of solvent are shown in Table 2. The free energies of activation show little dependence on isomer or solvent. Only a moderate dependence on the activation enthalpy is observed as a function of isomer (∼2−4 kcal/mol higher for **B** than for **A**) and solvent, but the activation entropy for the two isomers shows a clear trend (Table 2). We observe low or negative entropies of activation for isomer **A** (−7.5 to 1.4 cal mol^{-1} K^{-1}) and larger, positive values for **B** (7.4 to 11.4 cal mol^{-1} K^{-1}), which suggests a more organized transition state for the proton exchange in **A** compared to **B**.

$[Ni(P^{Cy}_2N^{Me}_2H)_2]^{2+}$ Isomers: Relative Free Energy. The NMR measurements along with previous experimental evidence[20,21] suggest that the intramolecular proton exchange is mediated by the metal center (Figure 2). To verify this mechanism and to address the potential impact of the overall molecular dynamics on the kinetics of the proton exchange, a series of *ab initio* calculations were performed. To reduce the computational cost, density functional theory (DFT) calculations were carried out on $[Ni(P^{Cy}_2N^{Me}_2)_2]^{2+}$, where the benzyl substituents of the N atoms were replaced by methyl groups.[30]

Ab initio geometry optimizations support the assignment of the geometries shown in **A**−**C** as the lowest-energy doubly protonated isomers (Figure 4). The relative free energies in

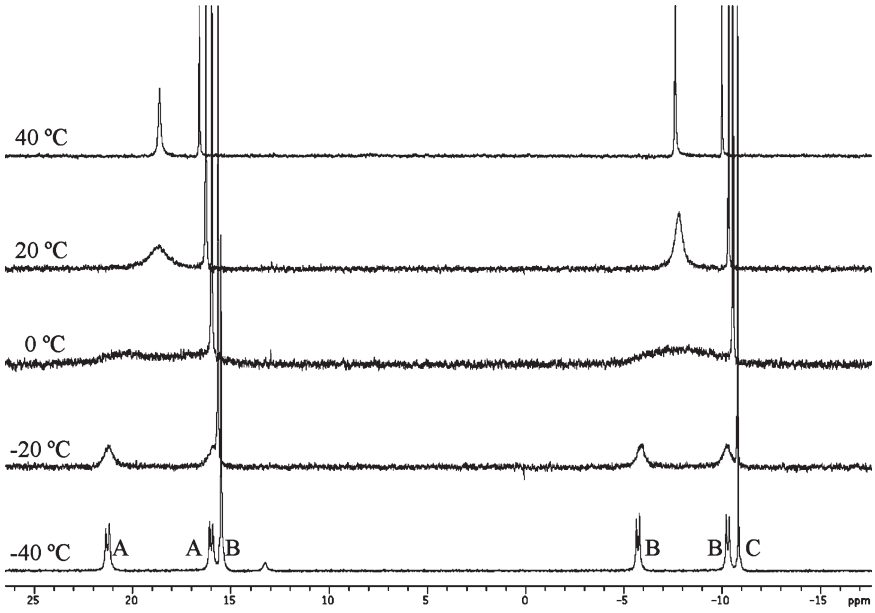

Figure 1. $^{31}P\{^{1}H\}$ NMR spectra of $[Ni(P^{Cy}{}_2N^{Bn}{}_2H)_2]^{2+}$ in CD_3CN as a function of temperature.

Table 1. Exchange Rate Constants (s^{-1}) for Intramolecular Proton Transfer for the A (Endo-Endo) and B (Endo-Exo) Isomers of $[Ni(P^{Cy}{}_2N^{Bn}{}_2H)_2]^{2+}$ as a Function of Temperature[a]

	isomer **A**			isomer **B**		
temp (K)	CD_3CN	acetone	CH_2Cl_2	CD_3CN	acetone	CH_2Cl_2
233	46	39	34	31	17	95
243	99	110	70	78	87	360
253	320	270	220	240	170	1 550
263	740	640	560	720	640	3 500
273	1 700	1 400	1 300	2 600	1 800	8 600
283	3 900	2 500	2 800	5 400	4 600	25 000
293	9 300	5 300	5 700	15 000	14 000	51 000
298	**12 000**	**6 600**	**8 600**	**27 000**	**16 000**	**84 000**
303	20 000	–	–	39 000	–	–
313	41 000	–	–	100 000	–	–
323	85 000	24 000	–	280 000	100 000	–

[a] Determined by line shape analysis of the $^{31}P\{^{1}H\}$ NMR spectra. Rate constants at 298 K are calculated from the resulting activation parameters.

acetonitrile are 1.6, 0.0, and 0.4 kcal/mol for isomers **A**, **B**, and **C**, respectively (Figure 4; a more complete ranking of the free energies of the different conformations of these three isomers is reported in Figure S5).

The six-membered rings containing endo protonated amines are found computationally to be in a boat conformation. Calculations indicate a significant hydrogen-bond-like d(Ni)→σ^*-(N−H) interaction,[31] with a hydrogen bond strength of approximately 7 kcal/mol between the Ni^0 and the NH proton for isomers **A** and **B**. The six-membered rings for the exo (pinched) moiety of isomers **B** and **C** are in chair conformations. In both isomers, the pinched moiety features a NH···N hydrogen bond with an estimated free energy of about 9−10 kcal/mol. The similarity of the hydrogen bond energies for the Ni^0···HN and

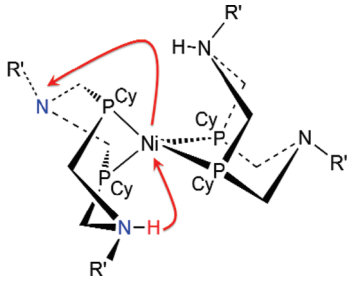

Figure 2. Simplified schematic representation of the proton exchange mechanism for the endo-endo isomer **A** based on the NMR data. Red arrows indicate the metal-mediated proton movement between two nitrogens. Figure 6 shows the complete mechanism for proton exchange.

N···HN hydrogen bonds results in species **A**−**C** having similar energies, consistent with the experimentally observed equilibrium between these three species. The six-membered rings containing non-protonated amines are all in chair conformations based on the computational analysis. Double protonation of a ligand is higly unfavorable. The lowest-energy isomer with a doubly protonated ligand lies 7 kcal/mol above **A**. This is consistent with experimental results, where double protonation of the same ligand is not observed for these complexes (see below).

Assessment of the Proton Exchange Pathways. To assess the possible paths for intramolecular exchange of the endo protons in isomers **A** and **B**, the free energy map for the proton movement in the all-boat conformer **A**″ (Figure 4) was calculated via gas-phase *ab initio* molecular dynamics. In this method, Newton's equations of motion are propagated in time according to forces obtained in the density functional theory electronic structure framework. In the following we will refer to free energies obtained via molecular dynamics as "classical" nuclei free energies. Although conformer **A**″ is not the lowest-energy endo-endo conformer (ΔG = 5.2 kcal/mol, Figure 4), it represents the best choice for studying the proton movement because of the symmetry introduced by all of the six-membered rings

being in the boat conformation. Indeed, each non-protonated pendant amine is in an optimal position for receiving the proton from a protonated amine. In addition, the use of conformer **A**″ avoids any complication due to the chair/boat conformational dynamics. The latter will be considered in a second stage (see below), where nuclear quantum (zero point energy, ZPE) effects will also be included.

The calculated classical nuclei free energy as a function of nitrogen/hydrogen coordination numbers (n_1 and n_2, see Computational Details) is shown in Figure 5. The map is symmetric with respect to the $y = x$ diagonal and features four distinct minima: the diproton species with a doubly protonated P_2N_2 ligand ($n_1 = 2$, $n_2 = 0$ or $n_1 = 0$, $n_2 = 2$), the diproton species with both the P_2N_2 ligands singly protonated ($n_1 = 1$, $n_2 = 1$), the proton-hydride species ($n_1 = 1$, $n_2 = 0$ or $n_1 = 0$, $n_2 = 1$), and the dihydride species ($n_1 = 0$, $n_2 = 0$).

Several important conclusions can be drawn from this map: (1) The proton exchange between the N atoms is mediated by the Ni atom. Indeed, the analysis of the molecular dynamics trajectory (Figure 5) shows that all of the possible diproton species are connected by a proton-hydride intermediate. (2) Double protonation of one ligand is disfavored by 4 kcal/mol for the **A**″ species, consistent with the B3P86 calculations. (3) The free energy surface is rather flat, which implies a very facile proton transfer from the pendant amine to the metal center. The overall classical nuclei activation free energy for moving a proton from N to Ni is about 7.0 kcal/mol. (4) Analysis of the metadynamics trajectory suggests that the hydride ligand easily moves from one face to another of the tetrahedron defined by the four phosphorus atoms. The activation barrier for this process is less than 3 kcal/mol (Figure S6). (5) Finally, the different proton-hydride species can also, in principle, be connected via a high-energy dihydride intermediate (ΔG = 11.0 kcal/mol). No other proton exchange pathways within 25 kcal/mol from the lowest-energy minima were found.

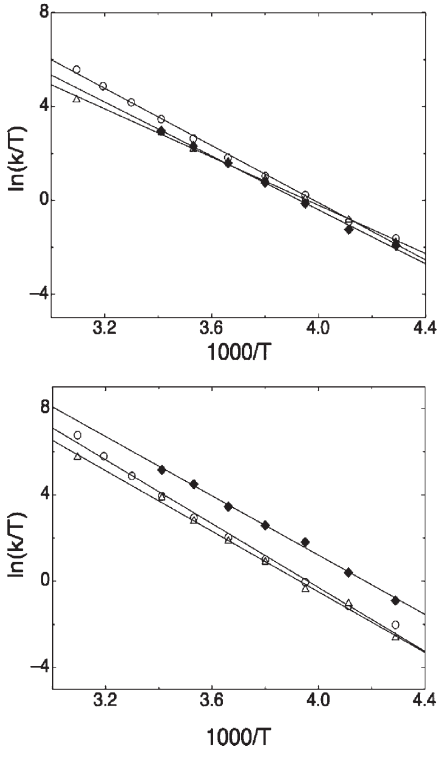

Figure 3. Eyring plots in CD_3CN (○), acetone (△), and dichloromethane (◆) for proton exchange in $[Ni(P^{Cy}_2N^{Bn}_2H)_2]^{2+}$, isomers **A** (top) and **B** (bottom).

High-Energy Pathways of Proton Exchange. Our computational studies suggested that intermediates involving either the Ni(IV) dihydride, $[(H)_2Ni(P^{Cy}_2N^{Bn}_2)_2]^{2+}$, or the Ni(0) doubly protonated ligand, $[Ni(P^{Cy}_2N^{Bn}_2H_2)(P^{Cy}_2N^{Bn}_2)]^{2+}$, were unlikely due to the high relative energies. To provide experimental confirmation, we prepared the H−D complex $[Ni(P^{Cy}_2N^{Bn}_2H)(P^{Cy}_2N^{Bn}_2D)]^{2+}$, because it results in unique ^{31}P resonances due to the proximity of the ^{31}P to an N−H or an N−D (see Figure S7 and Figure 5 of ref 21). If there is exchange of the H and D between ligands, the mechanism would involve one of two intermediates: a doubly protonated ligand, $[Ni(P^{Cy}_2N^{Bn}_2HD)(P^{Cy}_2N^{Bn}_2)]^{2+}$, or the hydride-deuteride, $[(H)(D)Ni(P^{Cy}_2N^{Bn}_2)_2]^{2+}$. Due to the unique resonances,

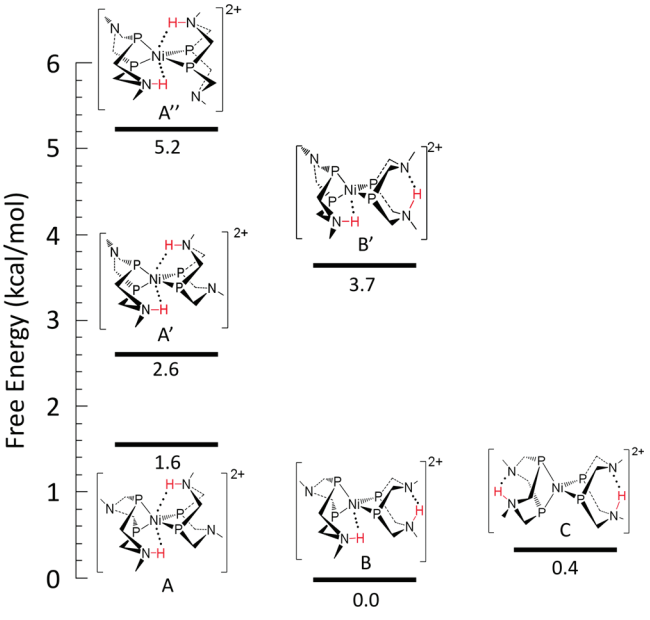

Figure 4. Ranking of the lowest free energy isomers of $[Ni(P^{Cy}_2N^{Me}_2H)_2]^{2+}$ calculated in acetonitrile at the B3P86/{Ni(SDD);P,N,C,H(6-31G*);(N-)H(6-31G**)} level of theory. For clarity, cyclohexyl groups on the P atoms are not shown.

Table 2. Activation Parameters for Proton Transfer in A (Endo-Endo) and B (Endo-Exo) Isomers of $[Ni(P^{Cy}_2N^{Bn}_2H)_2]^{2+a}$

	isomer **A**			isomer **B**		
	CD_3CN	acetone	CH_2Cl_2	CD_3CN	acetone	CH_2Cl_2
$\Delta H^{\ddagger}$ (kcal mol^{-1})	12.3 ± 0.3	10.0 ± 0.2	11.5 ± 0.4	14.8 ± 0.3	13.9 ± 0.2	13.7 ± 0.3
$\Delta S^{\ddagger}$ (cal mol^{-1} K^{-1})	1.4 ± 1.0	−7.5 ± 0.6	−1.9 ± 1.3	11.4 ± 0.9	7.4 ± 0.9	10.0 ± 1.1
$\Delta G^{\ddagger}$ (kcal mol^{-1})	11.9 ± 0.3	12.2 ± 0.2	12.0 ± 0.4	11.4 ± 0.3	11.7 ± 0.2	10.7 ± 0.3

[a] Determined from the rate constants shown in Table 1 and Figure 3.

dx.doi.org/10.1021/ja201838x |J. Am. Chem. Soc. 2011, 133, 14301–14312

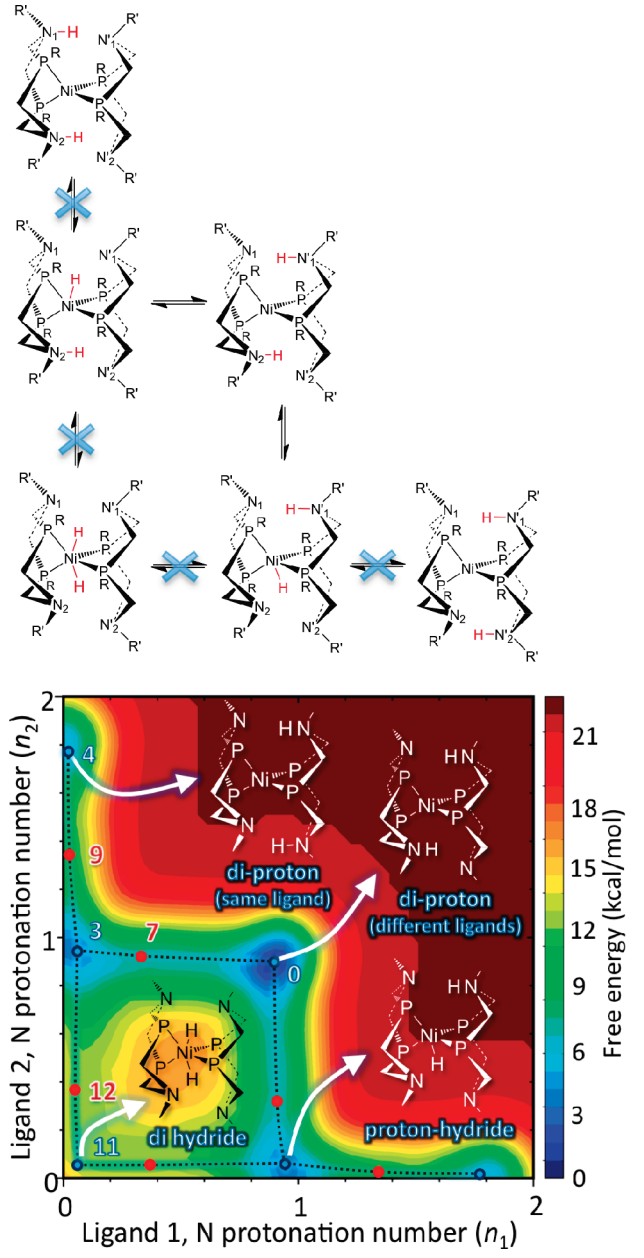

Figure 5. (Top) Schematic representation of the intramolecular proton exchange in the all-boat $[Ni(P^{Cy}_2N^{Me}_2H)_2]^{2+}$ (conformer **A**″, Figure 4), where each species maps to the corresponding lowest-energy isomer found in the *ab initio* meta-dynamics (lower panel). Equilibria leading to high-energy species whose presence is ruled out by NMR measurements are crossed out with an X. (Bottom) Corresponding free energy landscape projected onto the nitrogen/hydrogen coordination number of the two ligands. Local minima and transition states between them are marked with blue and red dots, respectively. Free energies at minima and transition states are also reported using the same colors. The dotted lines indicate lowest free energy pathways. Calculations were performed using PBE/{Ni(DZV2P);P,C,N,H(TZV2P)} gas-phase *ab initio* meta-dynamics simulations. For clarity, the 2+ charge on the Ni complex is not shown.

scrambling of the proton and deuteron between ligands could be observed using $^{31}P-^{31}P$ NMR exchange spectroscopy (EXSY).[32,33] While *intra*ligand exchange was observed (Figure S7, solid lines), no *inter*ligand exchange was observed over the temperature range where the individual ligand resonances are resolved (−65 to −10 °C). This confirms that each proton remains on the same ligand, providing strong evidence that neither the dihydride nor the diprotonated ligand species are intermediates in the proton transfer process (Figure 5, top). This is consistent with the interpretation that both the dihydride and the doubly protonated ligand species are significantly higher in energy than species with two singly protonated ligands.

Proton Exchange and Conformational Dynamics. The analysis reported above is strongly suggestive of a metal-mediated proton exchange mechanism. However, the picture emerging from the study of the all-boat endo-endo isomer is not complete. Indeed, all of the lowest-energy isomers feature the non-protonated pendant amine in a chair conformation. This finding suggests that, in the exchange pathway, a chair-to-boat conformational change should follow or precede the proton migration to the metal. We now analyze the effect of this conformational change as well as the proton movement in the overall transfer of the proton from one amine to the other.

To this end, we will not rely on *ab initio* simulations. Although they represent a powerful tool to carry out exhaustive searches for reaction channels, they are time-consuming, and it is impractical to use them to investigate all of the relevant isomers and conformers involved. In addition, they do not take nuclear quantum effects into account. In particular, inclusion of the vibrational ZPE is crucial to properly describe the relative energetics of the species involved in the proton movement, which are essential to properly describe the energetics of proton transfer. This contribution is missing in the Newtonian dynamics on which molecular dynamics is based. For these reasons, the structures of a series of species involved in the proton exchange dynamics as suggested by the *ab intio* simulations described above was refined by less time-demanding standard quantum chemistry geometry optimizations.

On the basis of the local minima and transition states located with the metadynamics simulation of the all-boat endo-endo **A**″ isomer (Figure 5), we have characterized the structure and energetics of all of the diproton species and hydride species involved in the hydrogen movement for all of the relevant endo-endo (**A**) and endo-exo (**B**) conformers at the DFT/B3P86 level of theory (Figures 6 and S8). Our computations indicate that the intramolecular proton exchange observed for isomers **A** and **B** involves three distinct processes: the transfer of a proton from N to Ni, migration of the resulting hydride ligand from one face to another of the tetrahedron defined by the four phosphorus atoms, and chair-to-boat conformational changes of the non-protonated rings.

The free energy barrier for the chair-to-boat isomerization of the non-protonated rings ranges from 7.7 to 10.7 kcal/mol, depending on the species. However, the corresponding barrier for the chair-to-boat isomerization of the pinched ring, which involves the loss of the N−H···N hydrogen bond, is about 16 kcal/mol. This result is consistent with the failure to observe intramolecular exchange of the pinched proton in isomer **B** with the endo proton. The chair-to-boat barriers for the unprotonated ligands of the proton-hydride species corresponding to **A** and **B** are 7.7 and 8.3 kcal/mol, respectively, about 2.4 kcal/mol smaller than the corresponding barriers for the protonated ligands of the diproton species. DFT/B3P86 calculations also confirm that the dihydride species, which has not been observed experimentally, is considerably higher in energy than the proton-hydride species.

In acetonitrile, the computed harmonic reaction free energy barrier for the N-to-Ni proton transfer is 5.1 and 5.3 kcal/mol for

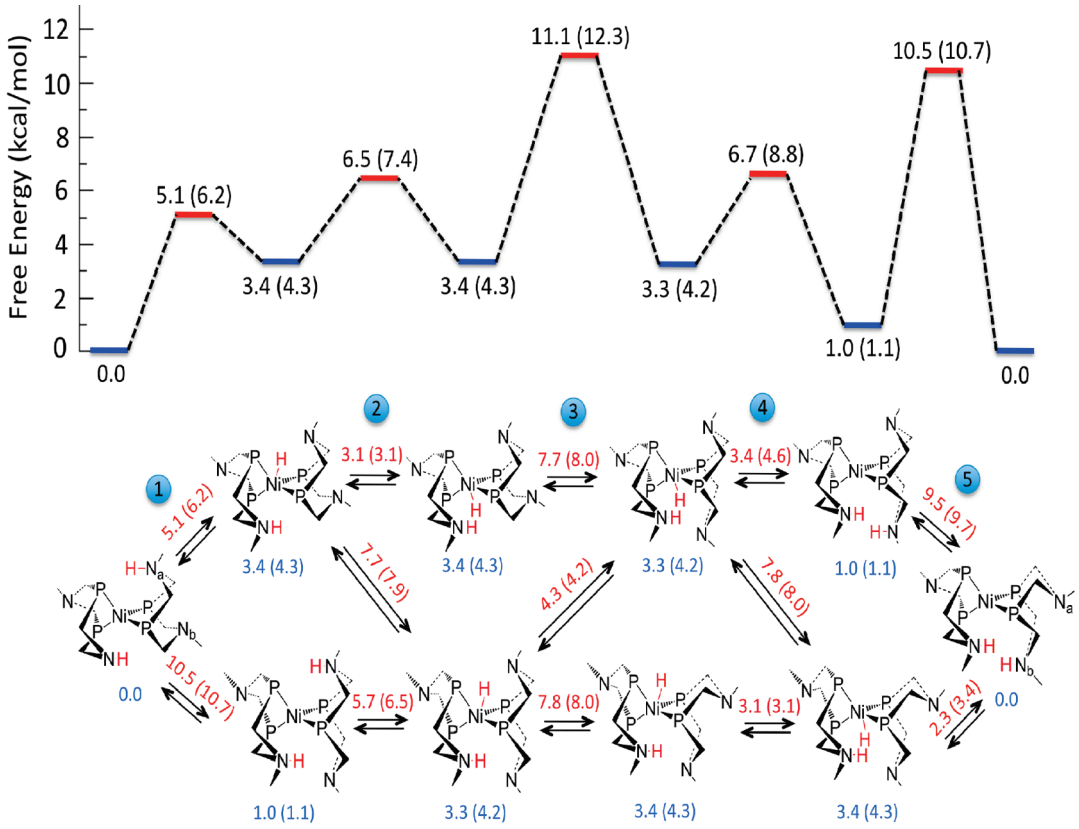

Figure 6. (Top) Free energy diagram for the exchange pathway indicated by numbers in the bottom scheme; reactant, product, and intermediates are indicated with blue lines placed on top of the corresponding species as reported in the bottom scheme, whereas transition states between them are reported as red lines (free energies are given with respect to the initial state). (Bottom) Full reaction mechanism of the intramolecular proton exchange for the endo-endo $[Ni(P^{Cy}{}_2N^{Me}{}_2H)_2]^{2+}$ isomer. Circled numbers indicate one of the eight possible shortest (five-step) exchange pathways. Blue numbers indicate the free energy of the species involved with respect to the initial isomer; red numbers indicate the activation free energy (in the direction of the arrow) of a given step. In both panels the numbers in parentheses indicate the free energy for the deuterated species. Calculations were carried out for acetonitrile solution at the B3P86/{Ni(SDD); P,N,C,H(6-31G*);(N-)H(6-31G**)} level of theory with harmonic estimates of thermal effects and entropy contributions using the CPCM solvation model. For clarity, the 2+ charge on the Ni complexes is not shown.

A and **B**, respectively. The barrier for the N-to-Ni proton transfer calculated for the all-boat conformer, **A**″, is 5.6 kcal/mol. This value is lower than the 7.0 kcal/mol obtained from the classical nuclei molecular dynamics in the gas phase (Figure 5). ZPE and different exchange and correlation functionals account for this difference.[35] The free energy barriers for hydride migration between faces of the tetrahedron range from 2.4 to 4.3 kcal/mol, depending on the chair/boat conformation of the non-protonated six-membered rings. Overall, the calculated activation free energy barriers for the N-to-Ni proton transfer and migration from one face to another are lower than the barrier for the chair-to-boat conformational change of the ring.

Kinetics of Proton Exchange. The intermediates involved in the proton exchange can be connected to each other in several ways, yielding the complete exchange mechanism shown in Figure 6 for isomer **A** and in Figure S8 for isomer **B**. From Figure 6 it is easy to see that the shortest exchange pathways involve five steps. There are a total of eight such pathways, which are the lowest-energy pathways; they differ only in the sequence of events.

As an example, consider the top pathway in the reaction diagram reported in Figure 6, whose steps are indicated by circled numbers. The first step consists of a proton transfer from N_a to Ni that leads to a proton-hydride intermediate (step 1). The hydride then migrates from one face to another of the tetrahedron defined by the four phosphorus atoms (step 2). These two processes are very fast. The third step is slower and involves a chair-to-boat transition of the ring containing the N_b atom (step 3). Finally, the proton transfers from Ni to N_b (step 4), and the ring containing N_a undergoes a boat-to-chair isomerization (step 5).

The other possible pathways can be derived starting from the pathway discussed above. For instance, the chair-to-boat isomerization (step 3) can take place before the hydride migration (step 2), or the boat-to-chair isomerization (step 5) can take place before the hydride-to-proton transformation (step 4). A chair-to-boat transition before the N-to-Ni proton transfer is equally possible.

The overall effective activation free energy, $\Delta G^{\ddagger}_{eff}$, can be derived from the (steady-state) effective kinetic constant obtained by solving the master equation of the network of reactions illustrated in Figures 6 and S8. Our calculations give a $\Delta G^{\ddagger}_{eff}$ at room temperature of about 10.7 and 10.3 kcal/mol for isomers **A** and **B**, respectively. Considering the slightly different chemical nature between the $[Ni(P^{Cy}{}_2N^{Me}{}_2)_2]^{2+}$ complex and $[Ni(P^{Cy}{}_2N^{Bn}{}_2)_2]^{2+}$, the agreement with the activation barrier determined from the NMR data in acetonitrile (11.9 and 11.4 kcal/mol respectively) is remarkable. The activation free

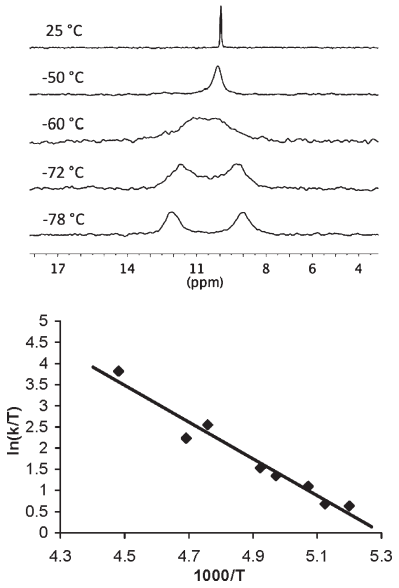

Figure 7. (Top) $^{31}P\{^{1}H\}$ NMR spectra of $[H\text{-}Ni(P^{Cy}{}_2N^{Bz}{}_2)_2]^+$ as a function of temperature. (Bottom) The Eyring plot of the chair-to-boat interconversion over the temperature range of −50 to −80 °C.

energies calculated in methylene chloride and acetone are very similar to those in acetonitrile, also in agreement with the corresponding experimental results. We note that the free energy barriers for proton exchange derived from each single five-step pathway are similar (about 11 kcal/mol, where differences among pathways are within 1.0 kcal/mol), and therefore all of them are potentially operative.

Chair/Boat Interconversion. Our computational results strongly suggest that the chair-to-boat interconversion is the rate-limiting step for intramolecular proton exchange, prompting additional experimental measurements. While we are unable to uniquely observe this interconversion for $[Ni(P^{Cy}{}_2N^{Bn}{}_2H)_2]^{2+}$, this process is observed for both $[Ni(P^{Cy}{}_2N^{Bn}{}_2)_2]^0$ and $[H\text{-}Ni(P^{Cy}{}_2N^{Bn}{}_2)_2]^+$ by $^{31}P\{^{1}H\}$ NMR (Figures S9 and 7, respectively). The free energies of activation for interconversion were found to be 7.7 kcal/mol for $[Ni(P^{Cy}{}_2N^{Bn}{}_2)_2]^0$ and 9.3 kcal/mol for $[H\text{-}Ni(P^{Cy}{}_2N^{Bn}{}_2)_2]^+$, in good agreement with computational predictions of 9.8 kcal/mol for $[Ni(P^{Cy}{}_2N^{Me}{}_2)_2]^0$ and 8.7 kcal/mol for $[H\text{-}Ni(P^{Cy}{}_2N^{Me}{}_2)_2]^+$. Additionally, the similarity in barriers for both hydride and non-hydride species provides indirect experimental evidence that the migration of the hydride about the Ni is facile.

Kinetic Isotope Effect (KIE). Deuterium exchange rates for $[Ni(P^{Cy}{}_2N^{Bn}{}_2D)_2]^{2+}$ were investigated experimentally, following the same procedure used in the proton exchange studies. The KIE was measured in CD_3CN and methylene chloride. For both solvents, k_H/k_D for **A** and **B** at 20 °C are 2.9 and 1.9, respectively.

Our calculations on $[Ni(P^{Cy}{}_2N^{Me}{}_2D)_2]^{2+}$ are consistent with the experimentally determined isotope effect, with theoretical KIEs of 2.4 and 1.8 for isomers **A** and **B**, respectively. Since the barriers for proton transfer are smaller than the barriers for the chair-to-boat conversion, it is of interest to analyze the origin of the observed isotope effect. To this end, it is useful to focus on just one of the possible exchange pathways, for instance the one marked with numbers from 1 to 5 in Figures 6 and S8. Since the chair/boat conversion steps (step 3 and 5) are slower than the proton transfer steps, the effective rate constant for the proton exchange is (see Experimental Section, eq 11)

$$k_{\text{eff}}^{(\text{f})} \approx \frac{k_1k_2k_3k_4k_5}{k_{-1}k_{-2}(k_{-3}k_{-4}+k_4k_5)} = K_{\text{eq}}^{(1)}K_{\text{eq}}^{(2)}\frac{k_3k_4k_5}{k_{-3}k_{-4}+k_4k_5} \quad (1)$$

where $k_{\text{eff}}^{(\text{f})}$ is the overall forward rate constant, k_n and k_{-n} are the forward and reverse rate constants of step n, and $K_{\text{eq}}^{(1)}$ and $K_{\text{eq}}^{(2)}$ are the equilibrium constants of steps 1 and 2 of Figures 6 and S8. From these figures it is evident that deuterium substitution predominantly affects the steps involving proton transfers between N and Ni (e.g., steps 1 and 4) and has little effect on the other steps (chair/boat interconversion and proton migration around the metal center). In particular, the first equilibrium constant $K_{\text{eq}}^{(1)}$ of the deuterated species is about 3.8 times smaller than the one for the non-deuterated species. This is a consequence of the different ZPE content associated with N−H and Ni−H bonds in the deuterated and non-deuterated species. A similar argument holds for the other possible pathways, but with a different magnitude. Therefore, the experimentally observed *kinetic* isotope effect is interpreted as being due to *equilibrium* isotopic effects on the steps involving proton transfers between Ni and N.

DISCUSSION

Mechanism of Proton Transfer. The pendant amines incorporated into the $[Ni(P^{R}{}_2N^{R'}{}_2)_2]^{2+}$ complexes[23−25] function as proton relays that facilitate intramolecular proton transfers in the catalytic oxidation and production of H_2. Catalytic activity for complexes containing positioned pendant amines occurs at much higher rates and/or lower overpotentials compared to catalysts that have no pendant amines, indicating their ability to lower barriers for these catalytic reactions.[16−26] An important aspect of many catalytic processes is the transfer of the proton between a metal center and an amine, and the results presented here provide detailed insight into this movement. Specifically, protons are transferred from the pendant amines to the metal center and out to the opposite pendant amine within the same ligand. The rate-limiting step in this process is the chair-to-boat conformational change of the non-protonated pendant amine. Our results show that several different pathways with comparable activation barriers connect the various species described above, as shown in Figure 6.

Up to 10 species can be involved in the intramolecular transfer of a proton from N_a to N_b. The numbered pathway in Figure 6 is representative of one of the shortest pathways for the endo-endo isomer A, which includes two proton transfers between N and Ni, one proton migration around the Ni face, and two chair-to-boat interconversions. Independent of which pathway is chosen, the chair-to-boat interconversion is the rate-limiting step in all cases, a result that was not obvious or anticipated. Particularly, the observed KIE would suggest that the rate-determining step involves the proton transfer. Because only the starting material and final products can be detected by NMR, and in this case multiple unobservable intermediate processes are encompassed in between, the computational analysis provides additional insight into the mechanism. While the rate-determining step does not involve the proton movement, the calculations show that the equilibration steps prior to the chair/boat interconversions (for

instance, step 1, Figure 6) are sensitive to deuteration, providing a reduction in rate (k_H/k_D = 2−3) similar to that observed experimentally. Additionally, direct measurement of the chair-to-boat interconversion in both $[Ni(P^{Cy}_2N^{Bn}_2)_2]$ and $[H\text{-}Ni(P^{Cy}_2N^{Bn}_2)_2]^+$ provides barriers similar to those observed computationally for $[Ni(P^{Cy}_2N^{Bn}_2H)_2]^{2+}$, providing experimental corroboration for the height of this barrier (8−11 kcal/mol).

Notably, neither the dihydride $[(H)_2Ni(P^{Cy}_2N^{Bn}_2)_2]^{2+}$ nor the doubly protonated ligand, $[Ni(P^{Cy}_2N^{Bn}_2H_2)(P^{Cy}_2N^{Bn}_2)]^{2+}$, are observed experimentally or participate as intermediates, as determined from EXSY NMR experiments (Figure S7). This is consistent with the high energies predicted computationally. Thus, the proton moves between N atoms on the same ligand, mediated by proton transfer to the metal, but not between ligands. This conclusion is consistent with the observation of an intramolecular exchange process in isomer **B** as well as for isomer **A**. It is interesting to note that both the Ni(IV) dihydride species and a doubly protonated $P^{Ph}_2N^{Bn}_2$ ligand (**3**) were observed for a related complex, $[Ni(P^{Ph}_2N^{Bn}_2)(dppp)]^{2+}$ (dppp = 1,2-bis(diphenylphosphino)propane), suggesting that the energetic landscape is relatively flat and highly tunable by modest changes in substituents.[22]

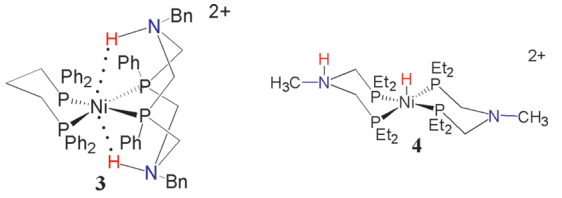

The present results also provide insight for the interpretation of previous studies. For instance, the addition of H_2 to $[Ni(PNP)_2]^{2+}$ (PNP = $Et_2PCH_2N(Me)CH_2PEt_2$), which contains pendant but unpositioned amines, gives the proton-hydride complex $[H\text{-}Ni(PNP)(PNHP)]^{2+}$ (**4**).[36] Facile intramolecular proton exchange, with rate constants on the order of 10^4 s^{-1}, was observed between the N−H and the Ni−H in this complex. A dihydride or dihydrogen intermediate was proposed for this intramolecular proton exchange.[36] The current results shown in Figure 5 place the dihydride complex 7 kcal/mol higher in energy than the proton-hydride, with a barrier of 12 kcal/mol. By extension, this suggests that, in the $[Ni(PNP)_2]^{2+}$ catalyst, the fast intramolecular proton transfer was from the Ni−H to the unprotonated amine, probably never going through a nickel dihydride species.

Rates of Intramolecular Proton Exchange and Implications for Catalysis. The rates of proton movement from one amine to another for isomers **A** and **B** are 10^4−10^5 s^{-1} at 25 °C, depending on the isomer and the solvent. The rates are consistently faster for **B** than for **A** in all solvents, by a factor of approximately 2 in acetone and acetonitrile and a factor of approximately 10 in methylene chloride. There is no clear dependence on solvent polarity, since rates are fastest in acetonitrile and slowest in acetone (the dielectric constants are 9.1, 21, and 37.5 for dichloromethane, acetone, and acetonitrile, respectively). The exchange rates for **B** are also not directly correlated to the dielectric constant, where rate constants are 5 times faster in methylene chloride than in acetone, and the rate in acetonitrile is 2 times faster than in acetone. The computational analysis suggests that the reduction in the barrier height for the chair-to-boat conformational change for the proton-hydride species (Figures 6 and S8) provides the largest contribution to the observed increase in rate for isomer **B**. The observed free energy barriers to intramolecular exchange also depend very little on solvent for both isomers, as shown in Table 2. The lack of significant solvent dependence for $\Delta G^{\ddagger}$ suggests that the rate-limiting step does not involve significant charge redistribution, consistent with a chair-to-boat transition as the rate-limiting step.

The rate constants of intramolecular proton transfer observed here are 100−1000 times larger than the rates of catalytic hydrogen production or oxidation, so proton transfer is clearly not the rate-limiting step in catalysis. Because the movement of protons to or from the metal is a necessary step in the catalytic cycle for both hydrogen production and oxidation, this work highlights the benefits of a carefully positioned proton relay in systems that have been thermodynamically matched to minimize the barrier to proton transfer. It is precisely because of the correct positioning that amine-to-metal proton transfer is not a rate-determining step; consequently, enhancing catalytic activity will require improvement of other proton transfers or electron transfers in the catalytic cycle.

It is interesting to compare the rates observed here to those for nitrogen-to-nitrogen proton transfers between organic amines and protonated amines, which typically occur at diffusion-controlled rates unless there is a significant steric influence. Because it is an intramolecular process, the rate of proton exchange in the $[Ni(P^{Cy}_2N^{R'}_2H)_2]^{2+}$ system can be comparable to the bimolecular self-exchange rate constants observed for amines, depending on the concentrations being considered (for example, 0.1 to 0.01 M amine would give first-order rate constants of 10^5 to 10^7 s^{-1}). While the mechanism for proton exchange for isomers **A** and **B** occurs in a multi-step pathway involving two proton transfers between the pendant amines and the metal, in addition to chair-to-boat conformational changes, these results highlight that the Ni-to-N proton transfer is not rate-limiting when amines are positioned correctly. In contrast, barriers to proton transfers between metal hydrides and metal anions[38−40] involve significantly higher barriers (and hence lower rates) compared to proton transfers between nitrogen atoms. While the proton transfers for the $Ni(P^R_2N^{R'}_2)_2$ catalysts between the pendant amines and the Ni are accompanied by a formal change in oxidation state of two units at Ni, these changes in electronic states do not limit fast proton transfer from amine to amine.

The mobility of the proton between the tetrahedral faces of the Ni atom in these small molecular catalysts may also point to flexibility of the location (or multiple locations) for the proton and hydrogen channels in the Ni−Fe hydrogenase enzyme.[9,12,41−43] If protons have a similar low barrier to mobility within the enzyme, a fluxional Ni hydride could enable the facile movement of the proton from one face of a four-coordinate Ni species to the other.[44] Several proton channels have been suggested on the basis of experimental[9,41] and computational studies,[42,43] all originating with the Ni, and the proposed hydrogen channel ends near a vacant coordination site on the Ni atom.[12] For the oxidation of hydrogen, the proton channel likely involves residue Glu-25 (*Desulfovibrio fructosovorans*), since hydrogen oxidation shuts down in its absence.[41] However, for proton reduction, one computational study found similar energies for two different proton transfer pathways, suggesting that different pathways may be used for proton reduction and hydrogen oxidation.[42] Multiple proton channels may imply that multiple proton positions on the metal

are easily accessible and may all function with similar rates due to fast intramolecular proton transfer.

In summary, the current studies demonstrate that proton transfers within $[Ni(P^{Cy}_2N^{R'}_2H)_2]^{2+}$ are significantly faster than catalysis and do not pose a barrier to catalytic activity. Importantly, they show how easily the proton can be moved from the Ni to the nitrogen (or *vice versa*) with the correct positioning of the amine, an essential step in the catalytic cycle for these catalysts, and more broadly to the dynamics of organometallic complexes with hydrogen bonds and enzymatic systems.[1,2,4,45−48] Investigations are ongoing to understand the mechanism of the pendant amines in the next step of catalysis: moving the proton into solution for catalyst regeneration.

CONCLUSIONS

Experimental and computational studies provide a detailed understanding of how the mobility of protons is accelerated by pendant amines in nickel catalysts for oxidation of H_2 and production of H_2. Protons are transferred intramolecularly very rapidly (10^4−10^5 s^{-1}) from one endo-positioned amine to another in the hydrogen oxidation catalyst, $[Ni(P^{Cy}_2N^{Bn}_2H)_2]^{2+}$, while exchange is not observed for protons positioned exo to the nickel. Computational models suggest a metal-mediated pathway involving proton transfers between the amine nitrogen and the nickel, rather than a direct nitrogen-to-nitrogen proton transfer. The major contributor to the barriers arises from chair/boat conformational interconversions of the six-membered rings of the diphosphine ligands, while migration around the Ni tetrahedron is facile. The fast rate of exchange is consistent with the low free energy for proton transfer, about 11−12 kcal/mol for both the endo-endo and the endo-exo isomers, essentially independent of solvent and supported by computational models. Due to the rapid intramolecular proton exchange, this family of catalysts for oxidation and production of H_2 may be considered as a metal center "immersed" in a cloud of protons, allowing multiple pathways for subsequent catalytic steps. More generally, the facile transfer of protons between the metal center and positioned bases/acids in the second coordination sphere of these $Ni(P^R_2N^{R'}_2)_2^{2+}$ complexes provides strong support for similar mechanisms proposed, but not directly observed, in enzymes.

EXPERIMENTAL SECTION

General. All samples were prepared under an N_2 atmosphere. Reaction solvents were dried using an Innovative Technologies Pure Solv solvent purification system. Acetone was not purified, but a fresh bottle was used for each sample preparation. CD_3CN was vacuum transferred from P_2O_5. All other chemicals were used as received.

Synthesis of $[Ni(P^{Cy}_2N^{Bn}_2)_2][BF_4]_2$. A procedure slightly modified from the previously reported synthesis was used.[21] Bis(hydroxymethyl)cyclohexylphosphine[20] (2.877 g, 0.016 mol) was dissolved in 50 mL of absolute ethanol in a Schlenk flask and heated to 70 °C. Neat benzylamine (1.78 mL, 0.016 mol) was added dropwise over 30 min, and the reaction was stirred for 12 h at 70 °C. The solvent was removed under reduced pressure to leave a sticky white solid, characterized by ^{31}P NMR as $P^{Cy}_2N^{Bn}_2$ (>95% pure). All of the crude ligand was added to $[Ni(CH_3CN)_6][BF_4]_2$[49] (2.04 g, 4.1 mmol) with 24 mL of acetonitrile; the reaction was stirred for 8 days at room temperature. The dark red solution was filtered and concentrated to 16 mL under reduced pressure. Vapor diffusion of Et_2O gave a dark purple crystalline product, $[Ni(P^{Cy}_2N^{Bn}_2)_2][BF_4]_2$ (1.92 g, 39% yield based on bis(hydroxymethyl)cyclohexyl phosphine). The spectral properties are consistent with those previously reported.[21]

Preparation of $[Ni(P^{Cy}_2N^{Bn}_2H)_2][BF_4]_2$. $[Ni(P^{Cy}_2N^{Bn}_2H)_2][BF_4]_2$ was prepared for NMR studies following a previously reported synthesis.[21] About 10−12 mg of $[Ni(P^{Cy}_2N^{Bn}_2)_2][BF_4]_2$ was dissolved into ∼1 mL of solvent, either methylene chloride, acetone, or acetonitrile-d_3, in an NMR tube under N_2 at room temperature. The samples were then purged for 3−5 min with hydrogen (ultrahigh purity, 99.999%) with an in-line drier (OxypurgeN) in series with an AT indicating cartridge (Alltech).

Preparation of $[Ni(P^{Cy}_2N^{Bn}_2D)_2][BF_4]_2$. $[Ni(P^{Cy}_2N^{Bn}_2D)_2][BF_4]_2$ was prepared as for $[Ni(P^{Cy}_2N^{Bn}_2H)_2][BF_4]_2$, in either CD_3CN or methylene chloride, with the modification of purging with D_2 (99.8%, Cambridge Isotopes), used as received, for 3−5 min.

Preparation of $[Ni(P^{Cy}_2N^{Bn}_2D)(P^{Cy}_2N^{Bn}_2H)][BF_4]_2$. $[Ni(P^{Cy}_2N^{Bn}_2D)(P^{Cy}_2N^{Bn}_2H)][BF_4]_2$ was prepared by the addition of HD gas (97%, Cambridge Isotopes) to the evacuated head space of a J. Young NMR tube (to minimize the amount of HD needed) containing a butyronitrile solution of $[Ni(P^{Cy}_2N^{Bn}_2)][BF_4]_2$ cooled to −78 °C.

Preparation of $Ni(P^{Cy}_2N^{Bn}_2)$. $[Ni(P^{Cy}_2N^{Bn}_2)_2][BF_4]_2$ (0.250 g, 0.020 mmol) was dissolved in 15 mL of acetonitrile. Hydrogen was purged through the solution for 10 min, followed by addition of 1,8-diazabicycloundec-7-ene (DBU, 0.07 mL, 0.45 mmol). After standing for 10 min, the solution was filtered, and the yellow precipitate was washed two times with 5 mL of acetonitrile to give the product as a yellow solid (200 mg, 94% yield). ^1H NMR (d_6-benzene): 1.09−1.80 (m, 46H), 2.48 (d, 8H) 2.82 (d, 8H), 3.73 (s, 8H) 7.13−7.26 (m, 24H). $^{31}P\{^1H\}$ NMR (d_6-benzene): 6.81 (s). NMR samples of $Ni(P^{Cy}_2N^{Bn}_2)_2$ were prepared by dissolving 10 mg of complex in 0.75 mL of butyronitrile. NMR data were collected from −103 to −81 °C.

Preparation of $[H\text{-}Ni(P^{Cy}_2N^{Bn}_2)_2]^+$. The reaction of $Ni(P^{Cy}_2N^{Bn}_2)_2$ (50 mg, 50 μmol) in 2 mL of THF with [HDMF][OTf][64] (12 mg, 50 μmol) in 0.5 mL of acetonitrile, followed by vapor diffusion of Et_2O, gave $[H\text{-}Ni(P^{Cy}_2N^{Bn}_2)_2][OTf]$ as orange crystals (45.6 mg, 80% yield). ^1H NMR (CD_3CN): −10.73 (pentet, J_{PH} = 19.9 Hz, 0.79H), 1.23−1.84 (br, 58H), 2.65 (d, 8H), 2.84 (d, 8H), 3.79 (s, 8H) 7.17−7.39 (br, 59H). $^{31}P\{^1H\}$ NMR (CD_3CN): 9.95 (s). The complex decomposes in solution to a paramagnetic species, presumably $[Ni(P^{Cy}_2N^{Bn}_2)_2]^+$. The impurity influences the integration of these peaks due to overlap. NMR samples of $[H\text{-}Ni(P^{Cy}_2N^{Bn}_2)_2][OTf]$ were prepared by dissolving 10 mg of complex in 0.75 mL of butyronitrile. NMR data were collected from −81 to −50 °C.

NMR Experiments. NMR experiments were run on Varian NMR systems at 300 or 500 MHz ^1H frequency, operated with a VNMRS console. Direct detect dual-band or OneNMR probes were used. Typical ^{31}P 90° pulses were ∼8 μs, and ^{31}P NMR spectra were collected with ^1H decoupling. Variable-temperature NMR data were collected from −103 to 50 °C, using either liquid nitrogen (lower than −60 °C) or an XRII852 sample cooler (FTS Systems, Stone Ridge, NY) (−60 to 20 °C) to achieve reduced temperature. 2D-EXSY[32,33] experiments were recorded at −65 to −10 °C using a standard phase-sensitive VNMRJ 2D NOESY pulse program with 128−256 increments, 16 scans per increment, and 200 ms mixing times.[50]

NMR Peak Fitting. The gNMR program was used for variable-temperature ^{31}P line shape analysis using a two-site exchange model.[51] Experimental spectra were processed within gNMR using a Lorentzian function with up to 6 Hz line broadening. Rates were determined by iteration of the simulated line widths, using both manual and gNMR algorithm methods. Visual inspection of the overlaid experimental and simulated spectrum was used to determine the best fit.

Eyring parameters were determined by fitting the rates as a function of temperature using eq 2:

$$k = \frac{k_B T}{h} e^{-\Delta H^{\ddagger}/RT} e^{\Delta S^{\ddagger}/R} \quad (2)$$

The data were fit using Profit, which allowed the application of individual error bars determined for each data point. Error bars were estimated to be 7−15% on the basis of visual inspection of the gNMR fits.

Computational Details. DFT calculations were carried out on $[Ni(P^{Cy}_2N^{Me}_2)_2]^{2+}$, where the benzyl substituents of the N atoms were replaced by methyl groups. This choice is validated by the very similar H_2 chemistry shared by $[Ni(P^{Cy}_2N^{Me}_2)_2]^{2+}$ and $[Ni(P^{Cy}_2N^{Bn}_2)_2]^{2+}$ (unpublished observations). To study the complexity of the intramolecular proton reorganization, a strategy based on two sets of *ab initio* calculations was adopted. Possible proton transfer pathways were explored on a chosen isomer via *ab initio* Born−Oppenheimer classical nuclei molecular dynamics simulations[52] along with enhanced sampling techniques[53,54] (see below). The structure of a series of species involved in the proton exchange dynamics as suggested by the *ab initio* simulations was refined for all of the possible isomers/conformers by less time-demanding standard quantum chemistry geometry optimizations. These include the diproton species, different possible proton-hydride intermediates, and transition states connecting them (Figures 6 and S8). For each isomer the chair/boat conformational change of the six-membered rings that incorporate the pendant amines was also characterized (Figures 6 and S8). All structures were optimized using all-electron DFT calculations with the B3P86 hybrid functional[55,56] along with the Stuttgart-Dresden relativistic ECP basis set (SDD) for Ni, 6-31G** for the acidic protons (i.e., the N−H protons), and 6-31G* for all of the other atoms. Harmonic vibrational frequencies were calculated at the optimized structures using the same level of theory to estimate the ZPE and thermal contributions (298 K and 1 atm) to the gas-phase free energy. Solvation free energies were then computed using a self-consistent reaction field model at the same level of theory as for the other steps. The Continuum Polarizable Conductor Model (CPCM) was used with Bondi radii.[57] All the calculations were carried out with Gaussian 09.[58]

The *ab initio* molecular dynamics simulations were carried out within the DFT framework using the hybrid Gaussian and plane waves method implemented in the CP2K code.[52] A double-ζ basis augmented with two sets of f-type, d-type, and p-type polarization functions was used for the 3s, 3p, 3d, and 4s orbitals of Ni (DZV2P), whereas a triple-ζ basis set augmented with two sets of d-type and p-type polarization functions was employed for the valence electrons of all of the other atoms (TZV2P basis set).[59] Norm-conserving pseudopotentials were used to treat core electrons of all of the atoms.[60] The electrostatic energy was calculated using an auxiliary plane wave basis set with a cutoff of 300 Ry in a 25 Å periodic cubic box.[52] The DFT calculations were carried out using the Perdew−Burke−Ernzerhof (PBE) functional.[61] The use of the PBE functional was dictated by computational cost of hybrid functionals, which make them unsuitable for long time scale *ab initio* simulations. Previous calculations showed that PBE yields only a slightly worse description of the energy of $Ni[P^R_2N^{R'}_2]_2^{2+}$ catalysts than the hybrid B3P86 functional.[35] To reconstruct the free energy landscape for the proton exchange at room temperature, an adaptive biasing force technique[53] based on a coarse-grained history-dependent dynamics (metadynamics) was employed. This approach is able to explore the free energy landscape in the space defined by a chosen set of degrees of freedom (collective coordinates), which describes the chemical process of interest. The evolution of the system at every step of the metadynamics is driven by the combined action of the thermodynamic force and a history-dependent force, which penalizes configurations in the collective variables space that have already been visited. The history-dependent potential is constructed as a sum of Gaussians centered on each value of the collective variable previously explored. The potential fills the minima of the free energy surface in time, and as the simulation proceeds, its sum converges to the free energy landscape as a function of the collective variables. In the present study, the number of hydrogen atoms coordinated to the nitrogen atoms of each ligand was employed to study the proton exchange along with the distance with the two exchanging hydrogens. A coordination coordinate[53] was introduced for each ligand, which assumes the value 0, 1, or 2, if none, one, or both nitrogens of a ligand are protonated, respectively. Gaussian functions of 0.1 kcal/mol height and 0.05 kcal/mol width were employed to bias this coordination number space.

As discussed in the text, the solvent has only a modest influence on the kinetics of proton exchange. Therefore, all of the molecular dynamics simulations have been performed in the gas phase starting from a relaxed structure of the all-boat $\mathbf{A}''$ species (see Figure 4). The molecule was left free to evolve at 25 °C for 2 ps, and then a metadynamics simulation was run for 30 ps, adding Gaussians every 25 fs. The equations of motion were propagated using a time step of 0.25 fs, controlling the temperature using a Nosé−Hoover chain of thermostats.[62]

This computational procedure has been shown to describe the Ni-based H_2 chemistry as well as coupled cluster CCSD[T] calculations.[35] In particular, B3P86, PBE, and CCSD[T] yield energy barriers for the proton transfer from the pendant amine to the metal center within about 1 kcal/mol.[35]

Kinetic Modeling. The time evolution of the population, p_i, of each of the 10 species involved in the exchange process (Figure 6) can be obtained from the following set of phenomenological first-order differential equations (master equation):[63]

$$\frac{dp_i(t)}{dt} = \sum_j [k_{ij}p_j(t) - k_{ji}p_i(t)] \tag{3}$$

where k_{ij} is the rate constant for the $j \rightarrow i$ reaction, and the summation runs over the 10 states. The master equation can be rewritten in the following compact matrix form:

$$\frac{d\mathbf{P}(t)}{dt} = \mathbf{WP} \tag{4}$$

where the elements of the matrix $\mathbf{W}$ are given by

$$W_{ij} = k_{ij} - \delta_{ij}\left(\sum_k k_{ki}\right) \tag{5}$$

The solution of eq 4 can be expressed in terms of the eigenvectors, $\phi_i = (\phi_i^{(1)}, \phi_i^{(2)}, ..., \phi_i^{(10)})$, and eigenvalues, λ_i, of the matrix $\mathbf{W}$:

$$p_i(t) = \sum_k c_k \phi_i^{(k)}\, e^{-\lambda_k t} \tag{6}$$

where the coefficients c_k are obtained under the detailed balance conditions

$$W_{ij}p_j^{(e)} = W_{ji}p_i^{(e)} \tag{7}$$

$p_i^{(e)}$ being the equilibrium (Boltzmann) population of the species i. It can be shown that there is an eigenvalue $\lambda_1 = 0$, whereas the others are all non-negative.[63]

The overall rate constant inferred from the NMR measurements can be obtained in the steady state regime, i.e., $t > 1/\lambda_2$, since λ_2 is the smallest nonzero eigenvalue, where the following effective rate law holds:

$$\frac{dp_{N_b}(t)}{dt} = k_{eff}^{(f)}p_{N_a}(t) - k_{eff}^{(b)}p_{N_b}(t) \tag{8}$$

Here $k_{eff}^{(f)}$ and $k_{eff}^{(b)}$ are the forward and backward effective rate constants, and $p_{N_a}(t)$ and $p_{N_b}(t)$ are the populations of the "initial" state (proton on nitrogen N_a) and "final" state (proton on nitrogen N_b, see Figure 6) at time t. Since the initial and final states are chemically identical, i.e., the population of the two states is equal, $k_{eff}^{(f)}$ and $k_{eff}^{(b)}$ are the same.

Finally, we briefly discuss the steady-state analytical solution of the master equation for a single five-step pathway (for instance, the one indicated by the circled numbers in Figure 6) employed for the analysis of the isotope effect. In this case the kinetic equations in the steady-state

regime are

$$\begin{aligned}
\frac{dp_2}{dt} &= k_1p_1 - (k_{-1} + k_2)p_2 + k_{-2}p_3 = 0 \\
\frac{dp_3}{dt} &= k_2p_2 - (k_{-2} + k_3)p_3 + k_{-3}p_4 = 0 \\
\frac{dp_4}{dt} &= k_3p_3 - (k_{-3} + k_4)p_4 + k_{-4}p_5 = 0 \\
\frac{dp_5}{dt} &= k_4p_4 - (k_{-4} + k_5)p_5 + k_{-5}p_6 = 0 \\
\frac{dp_6}{dt} &= k_5p_5 - k_{-5}p_6
\end{aligned} \tag{9}$$

where k_n and k_{-n} are the forward and backward rate constants for step n, which leads to

$$\frac{dp_6}{dt} = k_{\text{eff}}^{(f)}p_1 - k_{\text{eff}}^{(b)}p_6 \tag{10}$$

with effective (composite) rate constants

$$k_{\text{eff}}^{(f)} = \frac{k_1k_2k_3k_4k_5}{k_{-1}k_{-2}k_{-3}k_{-4} + k_{-1}k_{-2}k_{-3}k_5 + k_{-1}k_{-2}k_4k_5 + k_{-1}k_3k_4k_5 + k_2k_3k_4k_5} \tag{11}$$

and

$$k_{\text{eff}}^{(b)} = \frac{k_{-1}k_{-2}k_{-3}k_{-4}k_{-5}}{k_2k_3k_4k_5 + k_{-1}k_3k_4k_5 + k_{-1}k_{-2}k_4k_5 + k_{-1}k_{-2}k_{-3}k_5 + k_{-1}k_{-2}k_{-3}k_{-4}} \tag{12}$$

■ ASSOCIATED CONTENT

Supporting Information. (1) NMR spectra as a function of temperature in acetone and methylene chloride; (2) NMR line shape fits; (3) nonlinear Eyring plots for **A** and **B** in acetonitrile, methylene chloride, and acetone; (4) comprehensive free energy ranking of $[Ni(P^{Cy}_2N^{Me}_2H)_2]^{2+}$ isomers; (5) free energy for the hydride migration around the Ni atom in isomer $\mathbf{A}''$ as inferred from the metadynamics simulation; (6) reaction mechanism and energetic analysis for endo-exo isomer **B**; (7) 2D EXSY for HD exchange; (8) NMR spectra and Eyring plot for $[Ni(P^{Cy}_2N^{Bn}_2)_2]$ as a function of temperature; (9) complete ref 58; and (10) Cartesian coordinates of the optimized structure of all of the relevant species involved in the proton exchange process. This material is available free of charge via the Internet at http://pubs.acs.org.

■ AUTHOR INFORMATION

Corresponding Author

wendy.shaw@pnnl.gov; simone.raugei@pnnl.gov; morris.bullock@pnnl.gov.

■ ACKNOWLEDGMENT

We thank Dr. Don Camaioni and Dr. Roger J. Rousseau for useful discussions. This research was supported as part of the Center for Molecular Electrocatalysis, an Energy Frontier Research Center funded by the U.S. Department of Energy, Office of Science, Office of Basic Energy Sciences. W.J.S. was funded by the DOE Office of Science Early Career Research Program through the Office of Basic Energy Sciences. Computational resources were provided at W. R. Wiley Environmental Molecular Science Laboratory (EMSL), a national scientific user facility sponsored by the Department of Energy's Office of Biological and Environmental Research located at Pacific Northwest National Laboratory and the National Energy Research Scientific Computing Center (NERSC) at Lawrence Berkeley National Laboratory. Pacific Northwest National Laboratory is operated by Battelle for the U.S. Department of Energy. The authors thank Jeff London for assistance in designing the cover artwork.

■ REFERENCES

(1) Kaila, V. R. I.; Verkhovsky, M. I.; Wikstrom, M. *Chem. Rev.* **2010**, *110*, 7062–7081.
(2) Xu, J.; Voth, G. A. *Proc. Natl. Acad. Sci. U.S.A.* **2005**, *102*, 6795.
(3) Ketchem, R. R.; Hu, W.; Cross, T. A. *Science* **1993**, *261*, 1457.
(4) Roux, B. *Acc. Chem. Res.* **2002**, *35*, 366–375.
(5) Silverman, D. N.; McKenna, R. *Acc. Chem. Res.* **2007**, *40*, 669–675.
(6) Fontecilla-Camps, J. C.; Volbeda, A.; Cavazza, C.; Nicolet, Y. *Chem. Rev.* **2007**, *107*, 4273–4303.
(7) Nicolet, Y.; de Lacey, A. L.; Vernede, X.; Fernandez, V. M.; Hatchikian, E. C.; Fontecilla-Camps, J. C. *J. Am. Chem. Soc.* **2001**, *123*, 1596–1601.
(8) Volbeda, A.; Garcin, E.; Piras, C.; de Lacey, A. L.; Fernandez, V. M.; Hatchikian, E. C.; Frey, M.; Fontecilla-Camps, J. C. *J. Am. Chem. Soc.* **1996**, *118*, 12989–12996.
(9) Volbeda, A.; Charon, M.-H.; Piras, C.; Hatchikian, E. C.; Frey, M.; Fontecilla-Camps, J. C. *Nature* **1995**, *373*, 580–587.
(10) Armstrong, F. A.; Fontecilla-Camps, J. C. *Science* **2008**, *321*, 498–499.
(11) Leroux, F.; Dementin, S.; Burlat, B.; Cournac, L.; Volbeda, A.; Champ, S.; Martin, L.; Guigliarelli, B.; Bertrand, P.; Fontecilla-Camps, J.; Rousset, M.; Leger, C. *Proc. Natl. Acad. Sci. U.S.A.* **2008**, *105*, 11188–11193.
(12) Montet, Y.; Amara, P.; Volbeda, A.; Vernede, X.; Hatchikian, E. C.; Field, M. J.; Frey, M.; Fontecilla-Camps, J. C. *Nat. Struct. Biol.* **1997**, *4*, 523–526.
(13) Nicolet, Y.; Lemon, B. J.; Fontecilla-Camps, J. C.; Peters, J. W. *Trends Biochem. Sci.* **2000**, *25*, 138–143.
(14) Nicolet, Y.; Piras, C.; Legrand, P.; Hatchikian, C. E.; Fontecilla-Camps, J. C. *Structure* **1999**, *7*, 13–23.
(15) Peters, J. W.; Lanzilotta, W. N.; Lemon, B. J.; Seefeldt, L. C. *Science* **1998**, *282*, 1853–1858.
(16) Fraze, K.; Wilson, A. D.; Appel, A. M.; Rakowski DuBois, M.; DuBois, D. L. *Organometallics* **2007**, *26*, 3918–3924.
(17) Jacobsen, G. M.; Shoemaker, R. K.; McNevin, M. J.; Rakowski DuBois, M.; DuBois, D. L. *Organometallics* **2007**, *26*, 5003–5009.
(18) Jacobsen, G. M.; Yang, J. Y.; Twamley, B.; Wilson, A. D.; Bullock, M.; Rakowski DuBois, M.; DuBois, D. L. *Energy Environ. Sci.* **2008**, *1*, 167–174.
(19) Wilson, A. D.; Fraze, K.; Twamley, B.; Miller, S. M.; DuBois, D. L.; Rakowski DuBois, M. *J. Am. Chem. Soc.* **2008**, *130*, 1061–1068.
(20) Wilson, A. D.; Newell, R. H.; McNevin, M. J.; Muckerman, J. T.; Rakowski DuBois, M.; DuBois, D. L. *J. Am. Chem. Soc.* **2006**, *128*, 358–366.
(21) Wilson, A. D.; Shoemaker, R. K.; Miedaner, A.; Muckerman, J. T.; DuBois, D. L.; Rakowski DuBois, M. *Proc. Natl. Acad. Sci. U.S.A.* **2007**, *104*, 6951–6956.
(22) Yang, J. Y.; Bullock, R. M.; Shaw, W. J.; Twamley, B.; Fraze, K.; Rakowski DuBois, M.; DuBois, D. L. *J. Am. Chem. Soc.* **2009**, *131*, 5935–5945.
(23) Rakowski DuBois, M.; DuBois, D. L. *Acc. Chem. Res.* **2009**, *42*, 1974–1982.
(24) Rakowski DuBois, M.; DuBois, D. L. *Chem. Soc. Rev.* **2009**, *38*, 62–72.
(25) DuBois, D. L.; Bullock, R. M. *Eur. J. Inorg. Chem.* **2011**, *17*, 1017–1027.
(26) Kilgore, U.; Roberts, J.; Pool, D. H.; Appel, A.; Stewart, M.; Rakowski DuBois, M.; Dougherty, W. G.; Kassel, W. S.; Bullock, R. M.; DuBois, D. L. *J. Am. Chem. Soc.* **2011**, *133*, 5861–5872.

(27) Frey, M. *ChemBioChem* **2002**, *3*, 153–160.
(28) The small signal at ~13 ppm is due to the nickel hydride complex $[HNi(P^{Cy}_2N^{Bn}_2)_2]^+$, likely produced from reaction with residual water (unpublished results).
(29) Independent $^{31}P-^{31}P$ EXSY experiments confirmed that this exchange was intramolecular and not intermolecular (i.e., **A** does not transform to become **B**).
(30) This choice is validated by the very similar catalytic performance for H_2 oxidation shared by $[Ni(P^{Cy}_2N^{Me}_2)_2]^{2+}$ and $[Ni(P^{Cy}_2N^{Bn}_2)_2]^{2+}$ (unpublished observations).
(31) Brammer, L. *Dalton Trans.* **2003**, 3145–3157.
(32) Jeener, J.; Meier, B. H.; Bachmann, P.; Ernst, R. R. *J. Chem. Phys.* **1979**, *71*, 4546–4553.
(33) Perrin, C. L.; Dwyer, T. J. *Chem. Rev.* **1990**, *90*, 935–967.
(34) Dupuis, M.; Chen, S.; Raugei, S.; DuBois, D. L.; Bullock, R. M. *J. Phys. Chem. A* **2011**, *115*, 4861–4865.
(35) Chen, S.; Raugei, S.; Rousseau, R.; Dupuis, M.; Bullock, R. M. *J. Phys. Chem. A* **2010**, *114*, 12716–12724.
(36) Curtis, C. J.; Miedaner, A.; Ciancanelli, R.; Ellis, W. W.; Noll, B. C.; Rakowski DuBois, M.; DuBois, D. L. *Inorg. Chem.* **2003**, *42*, 216–227.
(37) Henry, R. M.; Shoemaker, R. K.; DuBois, D. L.; Rakowski DuBois, M. *J. Am. Chem. Soc.* **2006**, *128*, 3002–3010.
(38) Edidin, R. T.; Sullivan, J. M.; Norton, J. R. *J. Am. Chem. Soc.* **1987**, *109*, 3945–3953.
(39) Jordan, R. F.; Norton, J. R. *J. Am. Chem. Soc.* **1982**, *104*, 1255–1263.
(40) Kristjánsdóttir, S. S.; Norton, J. R. . In *Transition Metal Hydrides*; Dedieu, A., Ed.; VCH: New York, 1992; p 309−359.
(41) Dementin, S.; Burlat, B.; DeLacey, A. L.; Pardo, A.; Adryanczyk-Perrier, G.; Guigliarelli, B.; Fernandez, V. M.; Rousset, M. *J. Biol. Chem.* **2004**, *279*, 10508–10513.
(42) Galvan, I. F.; Volbeda, A.; Fontecilla-Camps, J. C.; Field, M. J. *Proteins: Struct., Funct. Bioinf.* **2008**, *73*, 195–203.
(43) Teixeira, V. H.; Soares, C. M.; Baptista, A. M. *Proteins: Struct. Funct. Bioinf.* **2008**, *70*, 1010–1022.
(44) Marr, A. C.; Spencer, D. J. E.; Schroder, M. *Coord. Chem. Rev.* **2001**, *219−221*, 1055–1074.
(45) Custelcean, R.; Jackson, J. E. *Chem. Rev.* **2001**, *101*, 1693–1980.
(46) Lee, D.-H.; Patel, B. P.; Clot, E.; Eisenstein, O.; Crabtree, R. H. *Chem. Commun.* **1999**, 297–298.
(47) Ott, S.; Kritikos, M.; Akermark, B.; Sun, L.; Lomoth, R. *Angew. Chem., Int. Ed.* **2003**, *43*, 1006–1009.
(48) Schwartz, L.; Eilers, G.; Eriksson, L.; Gogoll, A.; Lomoth, R.; Ott, S. *Chem. Commun.* **2006**, 520–522.
(49) Hathaway, B. J.; Underhill, A. E. *J. Am. Chem. Soc.* **1960**, 3705–3711.
(50) Thrippleton, M. J.; Keeler, J. *Angew. Chem., Int. Ed.* **2003**, *42*, 3938–3941.
(51) Budzelaar, P. H. M. *gNMR 5.0*; Adept Scientific: Herts, UK, 2006.
(52) VandeVondele, J.; Krack, M.; Mohamed, F.; Parrinello, M.; Chassaing, T.; Hutter, J. *Comput. Phys. Commun.* **2005**, *167*, 103–128.
(53) Laio, A.; Gervasio, F. L. *Rep. Prog. Phys.* **2008**, *71*, 126601.
(54) Laio, A.; Parrinello, M. *Proc. Natl. Acad. Sci. U.S.A.* **2002**, *99*, 12562–12566.
(55) Perdew, J. P. *Phys. Rev. B* **1986**, *33*, 8822.
(56) Becke, A. D. *J. Chem. Phys.* **1993**, *98*, 5648–5652.
(57) Bondi, A. *J. Phys. Chem.* **1964**, *68*, 441–451.
(58) Frisch, M. J. et al. *Gaussian 09*; Gaussian, Inc.: Wallingford, CT, 2009.
(59) VandeVondele, J.; Hutter, J. *J. Chem. Phys.* **2007**, *127*, 114105.
(60) Goedecker, S.; Teter, M.; Hutter, J. *Phys. Rev. B* **1996**, *54*, 8.
(61) Perdew, J. P.; Burke, K.; Ernzerhof, M. *Phys. Rev. Lett.* **1997**, *78*, 1396.
(62) Martyna, G. J.; Klein, M. L.; Tuckerman, M. *J. Chem. Phys.* **1993**, *97*, 9.
(63) van Kampen, N. G. *Stochastic Processes in Physics and Chemistry*, erd ed.; Elsevier: Amsterdam, 2007.
(64) Faviera, I.; Duñach, E. *Tetrahedron Lett.* **2004**, *45*, 3393–3395.